24th COBEM - 2017

24th ABCM International Congress of Mechanical Engineering
December 3-8, 2017, Curitiba, PR, Brazil

COBEM-2017-0414
STEPPED SINE AND MULTISINE SIGNAL EXCITATION FOR IDENTIFICATION IN A SMALL AMB TEST RIG

Diego Alejandro Godoy Diaz
Fernando Augusto de Noronha Castro Pinto
Thiago Gamboa Ritto
David Julian Gonzalez Maldonado
Federal University of Rio de Janeiro, Av. Horácio Macedo 2030 CT bloco i-130 LAVI, Rio de Janeiro.
dgodoy@ufrj.br
fcpinto@ufrj.br
tritto@poli.ufrj.br
davidjuliang@hotmail.com

Abstract. *Due to contactless ability and versatile excitation signals interface for identification purposes, Active Magnetic Bearings (AMBs) have become in the last 30 years an interesting tool for supporting and assessing heavy rotating machines, like turbochargers and generators. Pure harmonic signals for excitation are useful in identification because their energy is concentrated in the excited frequency, but nevertheless it demands a longer time than broadband signals. On the other hand, the limitation of the latter signals is the low Signal to Noise Ratio at high frequencies. The variables measured in AMBs are commonly the coil currents and shaft positions. In this paper, a comparison between experimental FRFs obtained using a Stepped sine and several Multisine input excitations in a small previously developed AMB test rig is made.*

Keywords: *Active Magnetic Bearing, System Identification, Broadband excitation*

1. INTRODUCTION

Active Magnetic Bearings are defined as mechatronic devices with a wide range of applications such as turbomachines, generators, food application pumps, underwater compressors, etc. The principle of levitating the shaft of a rotating machine is a very suitable solution when low maintenance, mechanical frictionless or uncontaminated environments are important requirements in a process (Schweitzer G. , 2002). Moreover, AMBs offer an online monitoring capacity that permits a reliable and safe operation. Besides the previous advantages, rotordynamic and seal parameters can be obtained by means of identification procedures.

For identification purposes in rotating machines applications, several excitation ways like impulsive inputs using instrumented hammers or pseudorandom signals performed by hydraulic shakers were implemented on field and laboratory tests. A detailed background of those methods are described by Nordmann (Nordmann, 1994) and Lee (Lee, 2006). In the last 25 years, excitation using electromagnetic devices became an interesting area of research and development due to their contactless advantage. Practically, any input signal can be used as excitation on this type of devices.

Most recent works (Hynynen, 2011) (Khader, 2015) conclude that if an adequate broadband excitation signal design is used, then an acceptable Signal to Noise Ratio (SNR) can be obtained reducing the time experiment consumption. This can be very essential when the time is a limitation in a specified test. Due to its worthy performance in presence of noise (Turkay & Usloy, 1988), identification is generally made in the frequency domain, that is, the use of frequency response function (FRF). Basically, this method consists in an excitation applied in a system while its inputs and outputs are measured by means of sensors or transductors. These measurements are treated and stored by a data acquisition system (DAQ) with a proper anti-alias filter, and then processed by an algorithm that computes their Discrete Fourier Transform, as shown in Figure 1. Finally, the ratio of the outputs and inputs are defined as the FRF. Nonlinear averaging methods using estimators also can be adopted in order to improve the SNR (Guillaume, 1988).

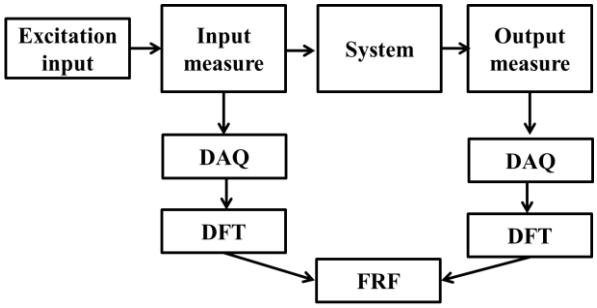

Figure 1. Block diagram for identification using FRF method (Nordmann, 1994)

The previous nonparametric method can be the basis of a parametric identification procedure, that involves fitting FRF's system curves in an established model. Regarding Magnetic Bearings, Gähler and Herzog (Gälher & Herzog, 1995) proposed several methods to obtain the parameters of a transfer function frame that represents the behavior of an AMB's plant.

2. AMB AND EXCITATION FOR IDENTIFICATION PROCEDURE

Basically, an AMB system can be split in four parts: A *rotor shaft*, that levitates due to a magnetic force exerted by an *electromagnetic actuator*, composed by set of bonded ferromagnetic sheets rolled up with coils in each leg with a controlled current provided by a set of power amplifiers. A *controller* with an implemented control algorithm decides the instantaneous current required in each coil in order to levitate the shaft, and a set of *position sensors* acts as the feedback control loop of the system (Schweitzer, Maslen, & Ma, 2009). A simplified block diagram is shown in Figure *2*.

As setpoint, generally the geometric bearing center is established. An excitation signal is added to the control signal making a perturbation in the system, and the measured signals are the coil currents u and the shaft positions y. Those measurements are contaminated by noise, denoted as n_u for the input and n_y for the output. The experiments of this paper were made with the rotor levitating, and for this analysis no rotational speed was applied. The FRFs obtained are related to the electromagnetic plant, whose includes the electromagnetic actuator, the rotor shaft and the position sensors.

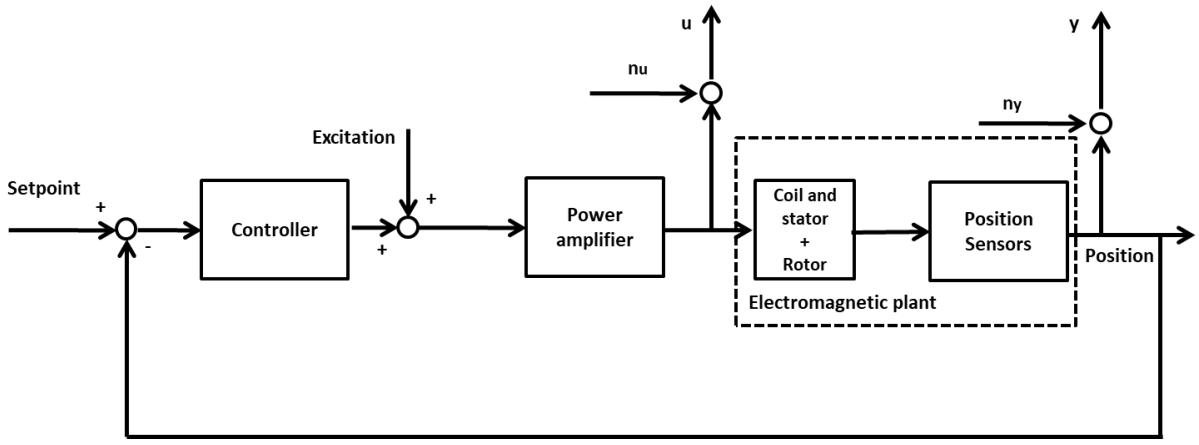

Figure 2. AMB system block diagram

In a coupled pair differential configuration, the coils of the pole pair in left-side and right-side carry the same current magnitude but in opposite way (i.e. $i_1 = -i_2, i_3 = -i_4$, see Figure 3) in order to close the magnetic circuit loop. Coupling the legs in pairs also allows to reduce the number of amplifiers, and therefore the number of electrical components and the control complexity.

A typical electromagnet configuration used in many test rigs is known as the differential configuration, since its control can be easily implemented (e.g. decoupled PID). One common example of the latter is the eight poles circular stator magnet, as shown in Figure 3, which can be set as a horizontal and a vertical differential configuration separately, if one assume that the magnetic flux coupling between those axes is negligible.

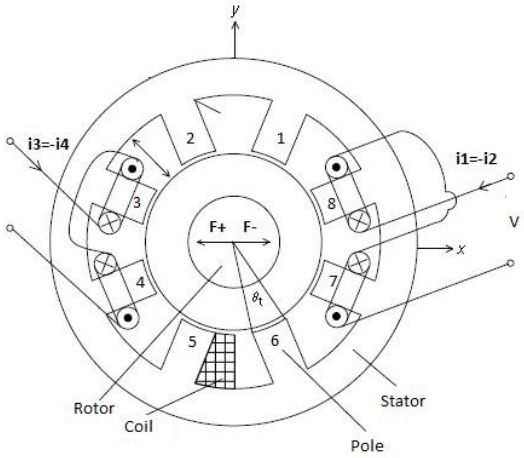

Figure 3. Eight poles circular electromagnet with coupled pairs configuration (modified) (Chiba, et al., 2005).

If the rotor displacements are small with respect to the air gap in the previously mentioned configuration, a linearized current model can be proposed establishing a base current operation i_0 (Chiba, et al., 2005). In this way, the current in the pole pair of each side depends of the base current and a perturbation current i_p, as shown in Figure 4. The perturbation current is composed by a control current i_x, defined by the controller (strongly necessary when the application includes an active magnetic bearing system) and a excitation current i_e related to the excitation signal S_e itself. Then, the current of the upper (i_1) and the lower (i_3) electromagnet can be expressed as:

$$i_1 = i_0 + i_p = i_0 + i_x + i_e \tag{1}$$

$$i_3 = i_0 - i_p = i_0 - i_x - i_e \tag{2}$$

The currents i_1 and i_3 can be measured by a set of current sensors, and the considered current in the identification procedure is the perturbation current i_p. Thereby, this perturbation current in one axis of an electromagnet using the linearized model can be obtained from the Equation (1) and (2), as follows:

$$i_p = \frac{i_1 - i_3}{2} \tag{3}$$

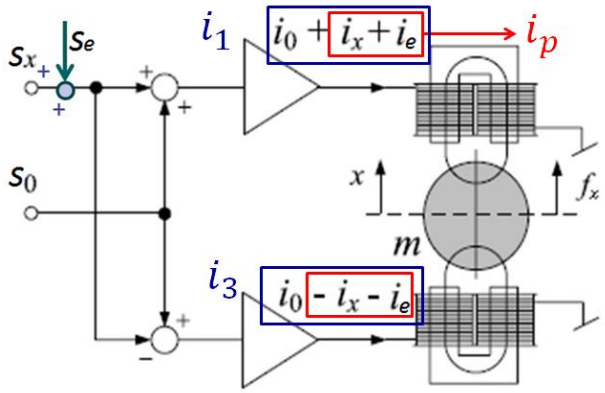

Figure 4. Electromagnet with horseshoe differential configuration (modified) (Schweitzer, et al., 2009).

2.1 Excitation signals

The excitation signals are an important stage of identification procedures due to their influence in the experimental system signal to noise ratio measurements. The most common signal is the known stepped sine, which have a good SNR since the energy is stored in only the excited frequency (Ljung, 1987). When a real test rig parameter identification process is made, a range of frequencies is desired. Thus, a sweep sine with discrete frequencies is an option to achieve the objective. One of the most important disadvantages of the previous signal is the time required to do the whole experiment. Another solution is using a multisine signal, that is, an overlap of several sines with different frequencies at the same time, which can be expressed as:

$$r_k = \sum_{i=1}^{N_f} A_k cos(2\pi f_k t + \phi_k) \quad (4)$$

where N_f is the number of individual overlapped stepped sines, A_k, f_k and ϕ_k are the amplitudes, frequencies and phases of $k-th$ harmonic respectively. As well as broadband signals, multisine signals split their energy into the excited frequencies, leading to a lower SNR, requiring techniques like averaging to increase it. Another complementary technique consists in manipulating the phases aiming to have a signal with low crest factor (Pintelon, et al., 2012). The crest factor of a discrete signal u, is defined as the ratio of the maximum absolute peak value u_{pk} and its respective discrete root mean square u_{rmse}, expressed as:

$$Cr(u) \equiv \frac{u_{pk}}{u_{rmse}} = \frac{max|u|}{\sqrt{\frac{1}{N}\sum_{i=1}^{N} u_i^2}} \quad (5)$$

For pure harmonic signals, the crest factor is *1.4*. In Figure 5 can be observed three types of multisine signal overlapping 50 frequencies with a flat unitary amplitude. The first one is a signal with no phase, which has a crest factor above *8.5*, being an inadequate choice in identification procedures. The second signal consist in random phases between 0 and 2π with uniform distribution and a crest factor of approximately *2.3*. This type of signal has better performance compared to the first signal, meaning less averages in order to increase the SNR. The phases of the last signal are obtained from the Scrhoeder's paper (Schroeder, 1970), and seems similar to a sweep signal when it has few harmonics. Its crest factor is about *1.9*, and leads into a good alternative when linearized models have to been excited for parameter identification techniques.

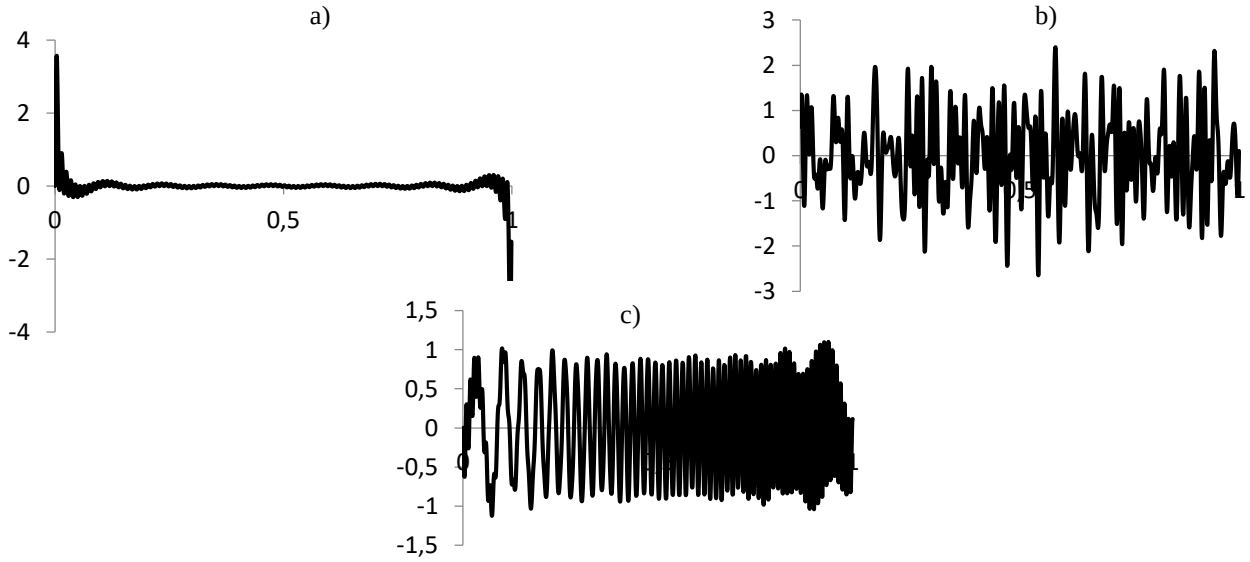

Figure 5. Excitation multisine signals $1-50\ Hz$ with $\Delta f = 1Hz$ and flat amplitude $A = 1\ V$ a) No phase, b) random phase and c) Schroeder phases.

2.2 FRF and estimators

The frequency response function (FRF) of a system for the frequency ω_k is defined as the ratio between the DFT of the output $\mathcal{Y}(\omega_k)$ and the input $\mathcal{U}(\omega_k)$, as follows:

$$\hat{\mathcal{G}}(\omega_k) = \mathcal{Y}(\omega_k)\mathcal{U}^{-1}(\omega_k) \quad (6)$$

Since measurements in an experiment are subjected to the presence of noise, a suitable estimator is necessary in order to obtain an appropriate frequency response function besides an adequate excitation signal. The use of an estimator implies more than one realization in order to average the FRFs. Several estimators for FRF applications are studied in detail by Guillaume (Guillaume, 1988) and Pintelon (Pintelon & Schoukens, 2012). For this paper, the *error in variables* $\hat{\mathcal{G}}_{EIV}$, *arithmetic mean* $\hat{\mathcal{G}}_{ARI}$, *logarithmic* $\hat{\mathcal{G}}_{LOG}$, the *autospectrum* estimator $\hat{\mathcal{G}}_{H1}$ and the *cross-spectrum based* estimator $\hat{\mathcal{G}}_{H2}$. The previous mentioned estimators can be expressed as:

$$\hat{\mathcal{G}}_{EIV}(\omega_k) = \left(\frac{1}{N_b}\sum_{l=1}^{N_b} \mathcal{Y}(\omega_k)^{(l)}\right)\left(\frac{1}{N_b}\sum_{l=1}^{N_b} \mathcal{U}(\omega_k)^{(l)}\right)^{-1} \tag{7}$$

$$\hat{\mathcal{G}}_{ARI}(\omega_k)\frac{1}{N_b}\sum_{l=1}^{N_b} \mathcal{Y}(\omega_k)^{(l)}\mathcal{U}^{-1}(\omega_k)^{(l)} \tag{8}$$

$$\hat{\mathcal{G}}_{LOG}(\omega_k) = exp\left(\frac{1}{N_b}\sum_{l=1}^{N_b} log\left(\hat{\mathcal{G}}(\omega_k)^{(l)}\right)\right) \tag{9}$$

$$\hat{\mathcal{G}}_{H_1}(\omega_k) = \left(\frac{1}{N_b}\sum_{l=1}^{N_b} \mathcal{Y}(\omega_k)^{(l)}\,\mathcal{U}^*(\omega_k)^{(l)}\right)\left(\frac{1}{N_b}\sum_{l=1}^{N_b} \mathcal{U}(\omega_k)^{(l)}\mathcal{U}^*(\omega_k)^{(l)}\right)^{-1} \tag{10}$$

$$\hat{\mathcal{G}}_{H_2}(\omega_k) = \left(\frac{1}{N_b}\sum_{l=1}^{N_b} \mathcal{Y}(\omega_k)^{(l)}\,\mathcal{Y}^*(\omega_k)^{(l)}\right)\left(\frac{1}{N_b}\sum_{l=1}^{N_b} \mathcal{U}(\omega_k)^{(l)}\mathcal{Y}^*(\omega_k)^{(l)}\right)^{-1} \tag{11}$$

where $\mathcal{U}^*(\omega_k)^{(l)}$ and $\mathcal{Y}^*(\omega_k)^{(l)}$ are the DFT complex conjugate of the input and output respectively and the superscript l denotes to the $l-th$ realization of the total number of realizations N_b.

3. AMB SMALL TEST RIG

A previous AMB small test rig was developed at the Acoustics and Vibrations Laboratory at the UFRJ by Siqueira (Siqueira, 2013) and then improved by Coelho (Coelho, 2016) (See Figure 6). In this test rig, the shaft is supported by an interaction between two eight heteropolar pole configuration stators and a decentralized PID algorithm implemented in a CPU controller with FPGA (cRio-9030). Four inductive sensors were installed in stator brackets in order to measure the shaft position and the control loop structure. Since the axial force is lower compared to the radial, the axial load is supported by a flexible coupling that also serves as torque transmission between a brushless motor and the shaft. The motor is controlled by an NI myRio 1900 development board. The most relevant features of the AMB system are summarized in Table 1.

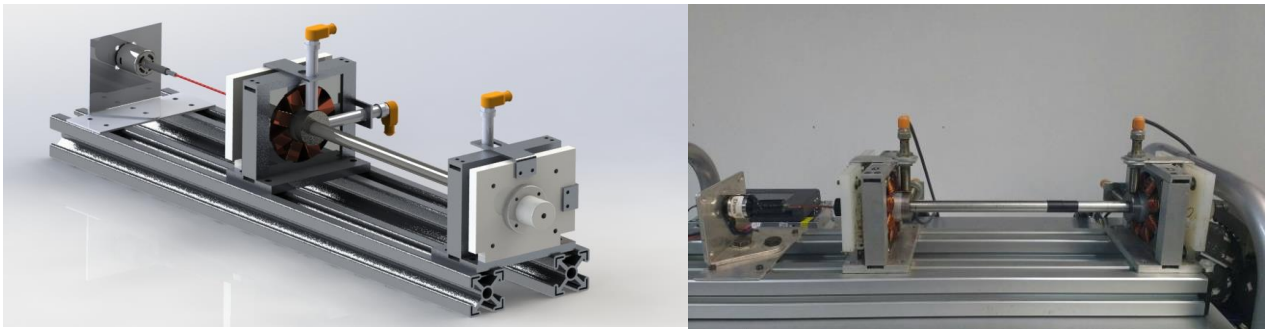

Figure 6. LAVI AMB small test rig: Conceptual design (left), prototype (right)

Table 1 Parameters of the small AMB test rig

Parameter	**Value**	**Un.**
Rotor mass	1	K_g
Shaft length	400	mm
Shaft diameter	14.28	mm
Journal diameter	36.4	mm
Bearing span between radial AMBs	315	mm
Distance between sensors	305	mm
Coil wire gauge	22	AWG
Turns per coil pair	260	
Bias current	1.0	A

Core thickness	0.5	mm
Core magnetic flux density saturation	1.7	T
Nominal air gap	1.0	mm
Pole area	235	mm^2
Negative position stiffness	-2.11e4	Nm^{-1}
Current stiffness	21.14	NA^{-1}

For the identification procedure, the algorithm of the previous AMB controller was modified to allow the excitation signal, adding as well a 16 bits 4- channel analog input module (NI 9223). A current sensor with a range of ±5A (ACS712) were installed in series of each current pair coil, in order to measure the currents trough each electromagnet pair. Therefore, using the linearized equations of the AMB model, the perturbation current of each axis has been computed.

In addition, a chassis for data acquisition (cDAQ 9178) was used with a dedicated computer algorithm in order to create the excitation signal and the acquisition of the current and position sensors. In the chassis were coupled two analog inputs modules (NI 9234) for the currents and one analog input module (NI 9239) for the position, and an analog output module for the excitation signals (NI 9263). A sample rate of 5 Khz was established for the acquisition and the excitation generation. The algorithm developed to acquire, compute the FFT and save those data was implemented in the Labview platform, and the post-processing part involving the estimator calculations was developed in a MATLAB script. The experiment diagram can be observed in Figure 7.

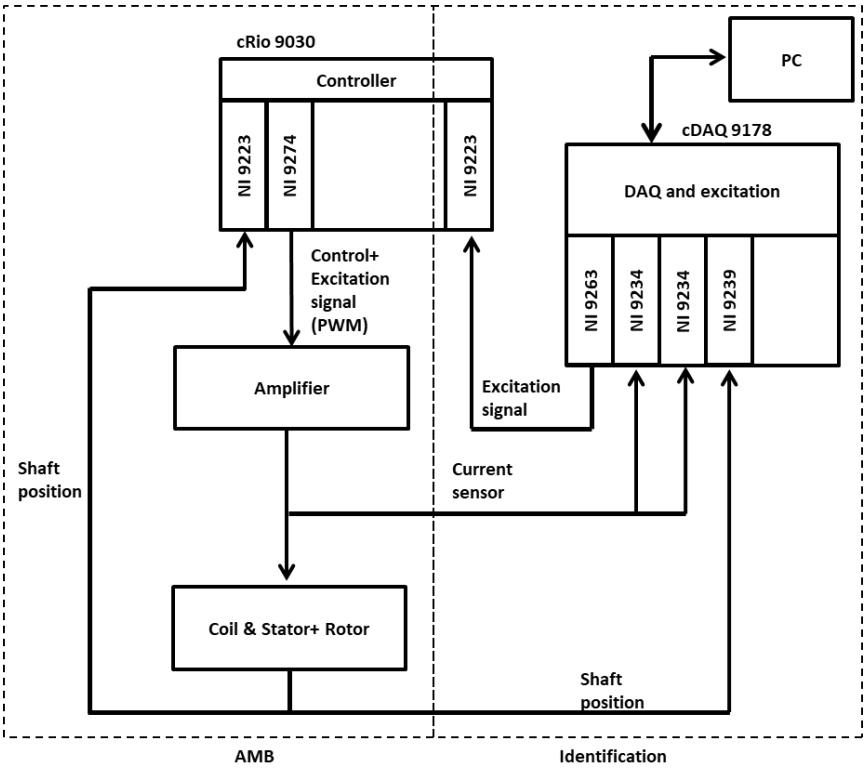

Figure 7. Small AMB test rig configuration for excitation and identification

4. EXPERIMENTAL RESULTS

Identification using the different broadband excitation signals previously mentioned in this paper was developed in the small test rig. The input of the system were the perturbation currents of vertical axis of each magnetic actuator, and the output were the vertical positions of the rotor measured in each side, as shown in Figure 8. That yields to a FRF matrix $\hat{\mathcal{G}} \in \mathbb{C}^{2x2}$. Since the number of the outputs are equal to two for this case, two different experiments were carried out with the aim of avoiding the singularities in the estimator matrices. In order to satisfy the latter requirement, the signal excitation was the same in the first experiment for the two inputs (i.e. $S_e[1 \quad 1]^T$), and for the second experiment the second input was negated (i.e. $S_e[1 \quad -1]^T$).

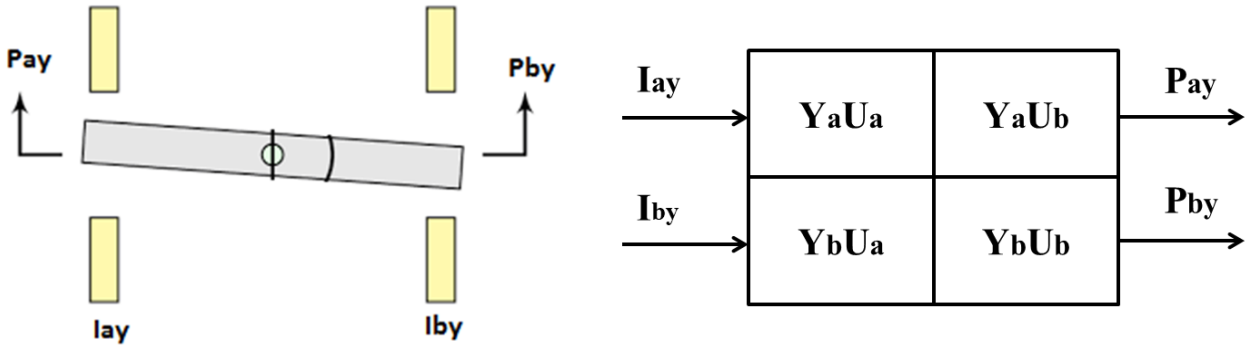

Figure 8. Identification sketch for vertical currents I_{ay}, I_{by} and vertical positions P_{ay}, P_{by}. Procedure diagram (left) and FRF scheme (right).

An example of input and output recorded measurements can be observed in Figure 9. In this case, an excitation using a multisine flat signal ($A_k = 100\ mV$) with random phases from 10 to 100 Hz increasing 1Hz was implemented. These measurements are related to the second experiment, where the second input signal is negated. It can be appreciated that the second input and output are not exactly the negative value of the first signal, since the AMB system has a feedback control and a coupled behavior, and in practice the stators are not strictly equal.

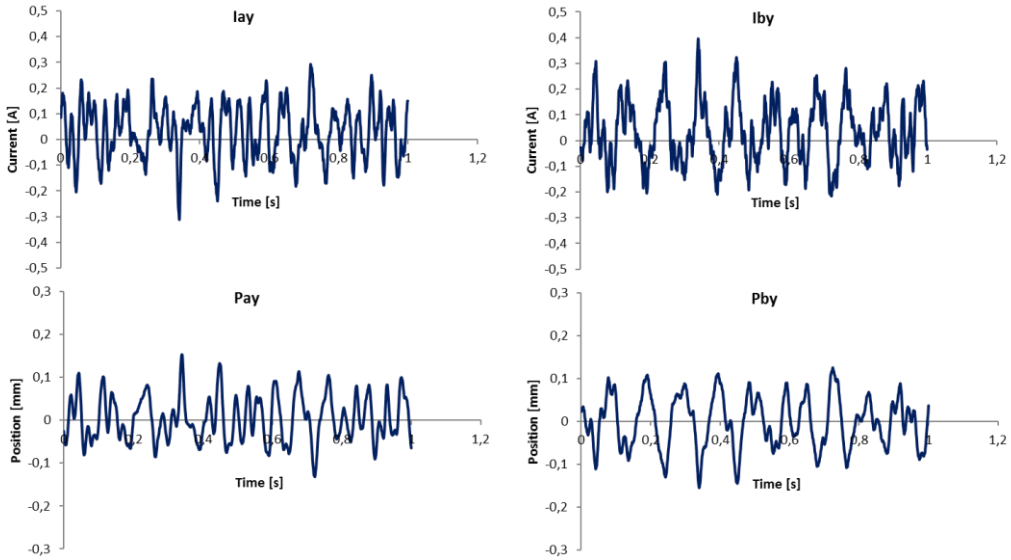

Figure 9. Measured currents and positions for a multisine excitation signal with random phase and frequency range 10-100 Hz, Δf=1Hz.

For the first results, the H_2 estimator was used, since the current sensors (input) showed a higher measurement noise than position sensors (output). In Figure 10 the different FRF responses can be observed, using a stepped sine (“Refe”) as a reference, because it concentrates the maximum energy in each excited frequency. The other broadband signals are the no phase (“Fas0”), random phase (“frand”) and Schroeder phases (“Schr”) multisine. It can be observed that Schroeder phases and random phases present a best approach to the reference signal. Conversely, the no phase multisine presents the most divergent approach. The G11, G12, G21, and G22 curves are a simplified simulated discrete-model using the geometrical AMB parameters.

Using as a flat multisine signal excitation with Schroeder phases from 10 to 100 Hz and increment of 1Hz, results have been obtained for the previous mentioned estimators, as shown in Figure 11, where one can observe that the closest approach curve to the reference (“Refe”) is the H_2. The most divergent curve is the logarithmic estimator (“LOG”). All estimators presents significant divergences above 60 Hz, especially in the coupled responses.

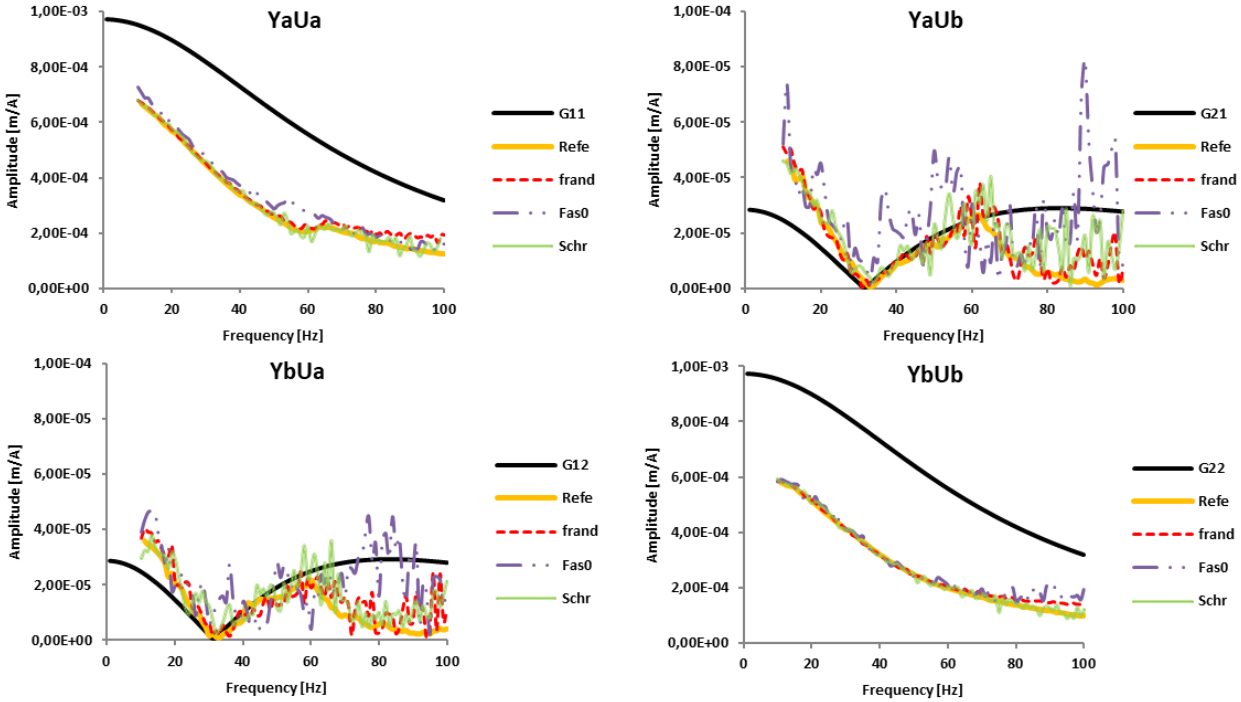

Figure 10. FRF of AMB system using different type of signal excitations using an estimator H_2 and 40 realizations, with frequency range 10- 100 Hz.

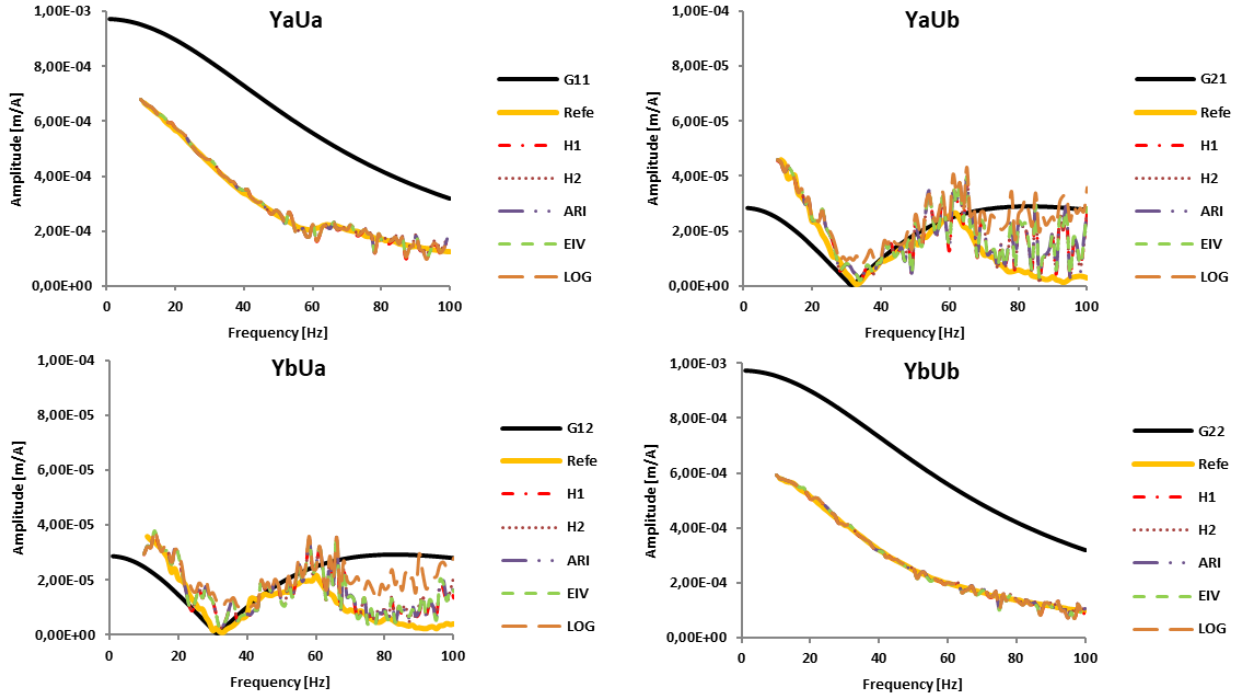

Figure 11. FRF of AMB system using different estimators and 40 realizations, a with frequency range 10- 100 Hz, Δf=1Hz.

5. CONCLUSIONS

Impulsive excitation signals like no-phase showed a lower approach since its energy is not well divided into the excited frequencies. Random phases showed a better performance and Schroeder phases had the best performance in the experimental results.

All coupled FRFs (YbUa and YaUb) presented divergences in all types of signal excitation, if compared with a direct FRFs (YaUa and YbUb). It is a topic to be studied in future works with more detail in order to have better responses, using different methods of excitation like optimized signals.

The simplified simulated model does not consider the current amplificator and magnetic actuator transfer function, and this could yield the divergence values in the coupled response beyond 60 Hz. A more robust model is being developed and its respective calibration procedure.

Regarding to the reference signal ("Refe") that consist in a stepped sine, the time consumption is quite greater than multisine signals, since it requires to be made individually in each frequency of excitation, also taking care with the transient plant time.

6. REFERENCES

Chiba, A., Fukao, T., Ichikawa, O., Oshima, M., Takemoto, M., & Dorrel, D. G. (2005). *Magnetic Bearings and Bearingless Drivers.* Great Britain: Elsevier Newnes.

Coelho, J. (2016). *Aspectos Mecânicos de Sistema de Mancais Magnéticos.* M.Sc. Dissertation. Rio de Janeiro: Federal University of Rio de Janeiro.

Gälher , C., & Herzog, R. (1995). Identification of magnetic bearing systems. *Mathematical and Computer Modelling of Dynamical Systems*, 29-45.

Guillaume, P. (1988, Junho). Frequency response measurements of multivariable systems using nonlinear averaging techniques. *IEEE Transactions on Instrumentation and Measurement, 47*(3), 706-800.

Hynynen, K. (2011). *Broadband Excitation in the System Identification of Active Magnetic Bearing Rotor Systems.* Ph.D. Thesis. Lappeenranta.: Lappeenranta University of Technology.

Khader, S. A. (2015). *System Identification of Active Magnetic Bearing for Commissioning.* M.Sc. Dissertation. Uppsala: Uppsala University.

Lee, C. W. (2006). Mechatronics in Rotating Machinery . *7th IFToMM-Conference on Rotor Dynamics*, (p. 16). Viena, Austria.

Ljung, L. (1987). *System identification: Theory for User.* New Jersey: Prentice Hall.

Nordmann, R. (1994). Identification Techniques in Rotordynamics. In *Diagnostics of Rotating Machines in Power Plants* (pp. 1-24). New York: Springer Verlag.

Pintelon, R., & Schoukens, J. (2012). *System identification. A Frequency Domain Approach. 2 Ed.* USA: Wiley.

Schroeder, M. (1970, Janeiro). Synthesis of low peak factor signals and binary sequences with low autocorrelation. *IEEE Transactions on Information Theory, 16*(1), 85-89.

Schweitzer, G. (2002). Active Magnetic Bearings – Chances and Limitations. Sydney: Proc. 6th Internat. IFToMM Conf. on Rotor Dynamics.

Schweitzer, G., Maslen, E. M., & Ma. (2009). *Magnetic Bearings: Theory, Design, and Application to Rotating Machinery.* New York: Springer.

Siqueira, R. (2013). *Projeto e Implementação de um Mancal Magnético Ativo com Controle por Modos Deslizantes.* M.Sc. Dissertation. Rio de Janeiro: Federal University of Rio de Janeiro.

Turkay, O., & Usloy, A. (1988). Frequency Versus Time Domain Parameter Estimation: Application to a Slot Milling Operation. *Mechanical Systems and Signal Processing, 2*(3), 265-277.

7. RESPONSIBILITY NOTICE

The author(s) is (are) the only responsible for the printed material included in this paper.